CONEM 2022
CONGRESSO NACIONAL DE ENGENHARIA MECÂNICA
TERESINA - PI

ABCM
XI CONGRESSO NACIONAL DE ENGENHARIA MECÂNICA
DE 07 A 11 DE AGOSTO DE 2022, TERESINA-PI, BRASIL

A PHENOMENOLOGICAL DESCRIPTION OF SHAPE MEMORY ALLOY FATIGUE

Vanderson M. Dornelas, vm.dornelas@mecanica.coppe.ufrj.br[1]
Marcelo A. Savi, savi@mecanica.ufrj.br[1]
Sergio A. Oliveira, sergio.oliveira@cefet-rj.br[2]
Pedro Manuel Calas Lopes Pacheco, pedro.pacheco@cefet-rj.br[2]

[1]Center for Nonlinear Mechanics, Department of Mechanical Engineering, Universidade Federal do Rio de Janeiro, COPPE, 21.941.972 Rio de Janeiro, RJ, Brazil
[2]Department of Mechanical Engineering, CEFET/RJ – Centro Federal de Educação Tecnológica Celso Suckow da Fonseca, 20.271.110 Rio de Janeiro, RJ, Brazil

Abstract: *Shape memory alloys (SMAs) belong to smart materials which can recover their shape when subjected to an appropriate thermomechanical field. These materials can be used in several applications considering different fields including biomedical, automotive, aerospace, civil engineering, and robotics, many of which involve cyclic loading conditions. In this regard, the fatigue phenomenon is an important subject that needs to be investigated. In general, SMAs exhibit two kinds of fatigue: functional fatigue related to the reduction of functional properties; and structural fatigue associated with the material failure due to the growth and propagation of microcracks. This contribution presents a numerical investigation of fatigue on shape memory alloys. A macroscopic three-dimensional constitutive model with internal variables is employed to describe functional and structural fatigue adopting a continuum damage perspective. The proposed model considers several phenomena related to SMAs, including transformation induced plasticity (TRIP), classical plasticity, phase transformation plasticity coupling, pseudoelasticity, and shape memory effect (SME), allowing an appropriate representation of the main aspects of the thermomechanical behavior of shape memory alloys. An equivalent critical damage is proposed to define the fatigue life of SMAs, considering different behaviors of martensitic and austenitic phases. In order to demonstrate the capabilities of the model, numerical simulations are compared with experimental data. Results show that the model responses are in close agreement with experimental data, including fatigue life predictions and loss of performance. In addition, numerical simulations considering different peak stress are proposed to evaluate the degradation of the functional parameters. Conclusions point out that the increase of the maximum stress promotes a reduction of the functional properties of the material due to the evolution of the TRIP strain and fatigue. These results are qualitatively similar to experimental results available in the literature, attesting to the model capability to describe the evolution of functional and structural fatigue in SMAs.*

Keywords: *shape memory alloys, functional fatigue, structural fatigue, constitutive model, numerical simulations.*

1. INTRODUCTION

Shape memory alloys are smart materials that have been used in many applications in different fields including biomedical, aerospace, automotive, among others, due to their remarkable properties related to martensitic phase transformations (Machado and Savi, 2003; Hartl and Lagoudas, 2007; Jani *et al.*, 2014; Nematollahi *et al.*, 2019). In many of these applications, SMAs are subjected to cyclic loading that induces fatigue. Therefore, fatigue of shape memory alloys is an important issue responsible for the loss of actuation performance and failure. SMA fatigue can be classified into two different ways: functional fatigue and structural fatigue, as suggested by Eggeler *et al.* (2004). Functional fatigue can be defined as the reduction of functional properties during cyclic loading. On the other hand, structural fatigue can be characterized by the accumulation of microstructural damage during cyclic loading that can cause failure, similar to other engineering materials.

The literature of SMA fatigue can be split into experimental and theoretical-numerical approaches. From the experimental point of view, different phenomena related to SMAs were analyzed to quantify the influence of functional and structural fatigue. For instance, Dornelas *et al.* (2021) proposed an experimental investigation to evaluate the main characteristics of functional and structural fatigue in nickel-titanium alloys (NiTi) subjected to different load conditions. Predki *et al.* (2006) studied the functional and structural fatigue of NiTi alloys subjected to torsion loads, showing that the fatigue occurs similarly as observed with axial loads. Zhao *et al.* (2020) conducted uniaxial fatigue tests to study the cyclic degradation of the one-way shape memory effect of nickel-titanium alloys. Results show a cyclic degradation of the shape memory effect, being dependent on stress rate and stress level, becoming more evident with the decrease of the

stress rate and the increase of the stress level. Other interesting studies available in the literature considering an experimental approach are Ramos *et al.* (2018), Jaureguizahar *et al.* (2018), Qiu *et al.* (2019), Qin *et al.* (2019), and Tyc *et al.* (2020).

Concerning the theoretical/numerical point of view, the constitutive modeling of shape memory alloys is an important subject that allows a proper understanding of fatigue phenomenon. In this regard, Hartl *et al.* (2014) developed a three-dimensional constitutive model based on the continuum damage mechanics, where the damage evolution is described through a function of both the stress state and the magnitude of the transformation strain, while the complete or partial nature of the transformation cycles is considered by experimental observations. Chemisky *et al.* (2018) proposed a three-dimensional constitutive model to describe functional and structural damage considering the coupling between the accumulation of damage and the transformation induced plasticity.

Mohammadzadeh *et al.* (2019) proposed a one-dimensional constitutive model to study the effects of the torsional low-cycle fatigue of superelastic SMAs considering high loading frequencies. Petrini and Bertine (2020) developed a three-dimensional phenomenological model to analyze the accumulation of inelastic strains due to fatigue and plasticity exploiting the pseudoelasticity and shape memory effect.

Dornelas *et al.* (2020) presented a three-dimensional constitutive model to describe functional fatigue in shape memory alloys considering a continuous damage perspective. This model is an extension of the one presented by Oliveira *et al.* (2016, 2018). Dornelas *et al.* (2021) incorporated structural damage to the previous model and proposed an equivalent critical damage to estimate the fatigue life of SMAs. Other constitutive models for the description of functional and structural fatigue on SMAs available in the literature are Barrera *et al.* (2014), Phillips *et al.* (2019), Liu *et al.* (2020a), and Liu *et al.* (2020b).

This paper presents a numerical investigation of functional and structural fatigue on shape memory alloys employing the three-dimensional model proposed by Dornelas *et al.* (2021). In order to verify the ability of the model to describe the SMA fatigue, a comparison with experimental data is conducted showing a good agreement including the fatigue life estimation. Afterward, numerical simulations are proposed to evaluate the degradation of the functional parameters during pseudoelastic cyclic loadings, including, the energy dissipation capacity, which can be calculated from the area surrounded by the stress-strain curve for each cycle (Kang *et al.*, 2012). The reduction of this functional parameter quantifies the loss of actuation performance over the cycles due to functional and structural fatigue. After this introduction, this paper is structured as follows. The constitutive model to describe functional and structural fatigue on shape memory alloys is summarized in Section 2. Section 3 presents the numerical simulations. The conclusions are presented in Section 4.

2. CONSTITUTIVE MODEL

This section summarizes the three-dimensional constitutive model proposed by Dornelas *et al.* (2020, 2021). The model is performed through the formalism of Generalized Standard Materials as proposed by Lemaitre and Chaboche (1990), and Halphen and Nguyen (1975). Under this assumption, the thermomechanical behavior of the material can be described by the Helmholtz free energy density, Ψ, and the pseudo-potential of dissipation, Φ. This approach assures that the second law of thermodynamics is satisfied, avoiding inconsistent behaviors. The procedure for obtaining the constitutive equations is discussed in more detail by Dornelas *et al.* (2020).

A macroscopic description based on local continuum damage perspective is proposed to describe functional and structural fatigue on shape memory alloys, using internal variables. Therefore, functional damage is represented by the loss of functional actuation, D_f; and structural damage is described by the degree of deterioration of the material, D_e. Based on that, consider that σ_{ij} is the stress tensor, ε_{kl}^{e} is the elastic strain tensor, and T is the temperature. In addition, four macroscopic phases are of concern, represented by their volume fraction: β^{+} and β^{-} are associated with detwinned martensitic variants (M^{+} induced by positive stress, and M^{-} induced by negative stress, respectively); β^{M} is associated with twinned martensite (M), and β^{A} is related to the austenitic phase (A). Since $\beta^{M} = 1 - \beta^{+} - \beta^{-} - \beta^{A}$, only three volume fractions are enough to describe the phase transformations. The description of classical plasticity is made through the plastic strain tensor, ε_{ij}^{p}, isotropic hardening, ϑ , and kinematic hardening ς_{ij}. On the other hand, transformation induced plasticity, defined as the plastic strain arising from phase transformation processes involving volume and/or shape changes without reaching the yield surface (Oliveira *et al.*, 2018), is described considering the TRIP strain, ε_{ij}^{trip}, and saturation variables for each phase, ξ^{+}, ξ^{-} and ξ^{A}. Under these assumptions, the thermomechanical behavior of SMAs, including functional and structural fatigue are presented in the sequence.

Stress–strain–temperature relation:

$$\sigma_{ij} = (1 - D_e)\left(E_{ijkl}\varepsilon_{kl}^{e}\right) + \alpha\omega_{ij}(\beta^{-} - \beta^{+}) - \Omega_{ij}(T - T_0) \tag{1}$$

Evolution equations for the volume fractions:

$$\dot{\beta}^{+} = \frac{1}{\eta^{+}}\left[\alpha\Gamma + \left(1 - D_f\right)\Lambda + P^{+} - \alpha_{ijkl}^{h} r_{kl}\Omega_{ij}(T - T_0) - \eta^{I} K\vartheta - \eta_{ij}^{K}\frac{\varsigma_{ij}}{H} - \kappa_{\pi}^{+}\right] + \kappa_{\chi}^{+} \tag{2}$$

$$\dot{\beta}^{-} = \frac{1}{\eta^{-}}\left[-\alpha\Gamma + \left(1 - D_f\right)\Lambda + P^{-} + \alpha_{ijkl}^{h} r_{kl}\Omega_{ij}(T - T_0) - \eta^{I} K\vartheta - \eta_{ij}^{K}\frac{\varsigma_{ij}}{H} - \kappa_{\pi}^{-}\right] + \kappa_{\chi}^{-} \tag{3}$$

$$\begin{aligned}\dot{\beta}^{A} = \frac{1}{\eta^{A}}\Big[&\left(1 - D_f\right)\Lambda^{\aleph} + P^{A} + \varepsilon_{ij}^{e}\left(\Omega_{ij}^{A} - \Omega_{ij}^{M}\right)(T - T_0) - \frac{1}{2}(K^{A} - K^{M})\vartheta^{2} - \\ &- \left(\frac{1}{2H^{A}} - \frac{1}{2H^{M}}\right)\varsigma_{ij}\varsigma_{ij} + \eta^{I} K\vartheta + \eta_{ij}^{K}\frac{\varsigma_{ij}}{H} - \kappa_{\pi}^{A}\Big] + \kappa_{\chi}^{A}\end{aligned} \tag{4}$$

Evolution equations for plasticity:

$$\dot{\varepsilon}_{ij}^{p} = \gamma\frac{\hat{\sigma}_{ij} - \varsigma_{ij}}{\left\|\hat{\sigma}_{ij} - \varsigma_{ij}\right\|} \tag{5}$$

$$\dot{\vartheta} = \sqrt{\frac{2}{3}}\gamma + \eta^{I}\left(\dot{\beta}^{+} + \dot{\beta}^{-} - \dot{\beta}^{A}\right) \tag{6}$$

$$\dot{\varsigma}_{ij} = \frac{2}{3}H\dot{\varepsilon}_{ij}^{p} + \eta_{ij}^{K}\left(\dot{\beta}^{+} + \dot{\beta}^{-} - \dot{\beta}^{A}\right) \tag{7}$$

Evolution equations for TRIP:

$$\dot{\varepsilon}_{ij}^{trip} = 2\sigma_{ij}\left\{(M_{13}\beta^{+} + M_{31}\beta^{A})\dot{\beta}^{+} + (M_{32}\beta^{-} + M_{23}\beta^{A})\dot{\beta}^{-} + [M_{43}\beta^{A} + M_{34}(1 - \beta^{+} - \beta^{-} - \beta^{A})]\dot{\beta}^{A}\right\} \tag{8}$$

$$\dot{\xi}^{+} = \left|\dot{\beta}^{+}\right|; \quad \dot{\xi}^{-} = \left|\dot{\beta}^{-}\right|; \quad \dot{\xi}^{A} = \left|\dot{\beta}^{A}\right| \tag{9}$$

Evolution equation for functional damage:

$$\dot{D}_f = (C_1 + C_2\Gamma^{\sigma})^{C_3}\left(\left|\dot{\beta}^{+}\right| + \left|\dot{\beta}^{-}\right| + \left|\dot{\beta}^{A}\right|\right) \tag{10}$$

Evolution equation for structural damage:

$$\dot{D}_e = (C_4 + C_5\Gamma^{\sigma})^{C_6}\left|\dot{\varepsilon}_{ij}^{e}\right| + (C_7 + C_8\Gamma^{\sigma})^{C_9}\left|\dot{\varepsilon}_{ij}^{p}\right| \tag{11}$$

Yield surface and its conditions:

$$f = \left\|\hat{\sigma}_{ij} - \varsigma_{ij}\right\| - \sqrt{\frac{2}{3}}(\sigma_Y - K\vartheta) \tag{12}$$

$$\gamma \geq 0; \;\; f \leq 0 \text{ and } \gamma f = 0; \;\; \gamma\dot{f} = 0 \text{ if } f = 0 \tag{13}$$

In these equations, $\Gamma = \frac{1}{3}\varepsilon_{kk}^{e} + \frac{2}{3}\sqrt{3J_2^{e}}\,\mathrm{sign}(\varepsilon_{kk}^{e})$ is the equivalent strain field that combines volumetric, ε_{kk}^{e}, and deviatoric, J_2^{e}, effects; $\kappa_{\pi}(\beta^{+}, \beta^{-}, \beta^{A})$ and $\kappa_{\chi} = \kappa_{\chi}\left(\dot{\beta}^{+}, \dot{\beta}^{-}, \dot{\beta}^{A}\right)$ are related to phase transformation constraints being defined from sub-differential of indications functions. The internal dissipation during the phase transformation is represented by the parameters $\eta^{m}(m = +, -, A)$ as follows:

$$\begin{cases}\eta^{\pm} = \eta_{L}^{\pm} & \text{if } \dot{\Gamma} > 0 \\ \eta^{\pm} = \eta_{U}^{\pm} & \text{if } \dot{\Gamma} < 0\end{cases}; \begin{cases}\eta^{A} = \eta_{L}^{A} & \text{if } \dot{\Gamma} > 0 \\ \eta^{A} = \eta_{U}^{A} & \text{if } \dot{\Gamma} < 0\end{cases} \tag{14}$$

The parameters η_L^+, η_L^-, η_U^+, η_U^-, η_L^A and η_U^A are obtained considering fourth-order tensors, assuming the isotropy of the material. Thus, consider a general formulation defined from the symbol $\mathcal{N}$ that represents each of the previous parameters, as follows:

$$\begin{cases}(\mathcal{N}) = r_{ij}(\widetilde{\mathcal{N}})_{ijkl}r_{kl} \text{ if } \Gamma^\sigma \neq 0 \\ (\mathcal{N}) = (\mathcal{N})_N \text{ otherwise}\end{cases} \tag{15}$$

where $(\widetilde{\mathcal{N}})_{ijkl}$ is given by:

$$(\widetilde{\mathcal{N}})_{ijkl} \equiv \begin{bmatrix} (\mathcal{N})_N & (\mathcal{N})_N-(\mathcal{N})_S & (\mathcal{N})_N-(\mathcal{N})_S & 0 & 0 & 0 \\ (\mathcal{N})_N-(\mathcal{N})_S & (\mathcal{N})_N & (\mathcal{N})_N-(\mathcal{N})_S & 0 & 0 & 0 \\ (\mathcal{N})_N-(\mathcal{N})_S & (\mathcal{N})_N-(\mathcal{N})_S & (\mathcal{N})_N & 0 & 0 & 0 \\ 0 & 0 & 0 & 2(\mathcal{N})_S & 0 & 0 \\ 0 & 0 & 0 & 0 & 2(\mathcal{N})_S & 0 \\ 0 & 0 & 0 & 0 & 0 & 2(\mathcal{N})_S \end{bmatrix} \tag{16}$$

where $(\mathcal{N})_N$ and $(\mathcal{N})_S$ represents normal and shear components of the specific parameter, respectively. Moreover, Γ^σ is the equivalent stress field; its definition is similar to the one employed for the equivalent strain field.

In addition, α_{ijkl}^h is a fourth-order tensor that controls the stress-strain hysteresis loop width represented by a matrix (assuming the hypothesis of symmetry), considering the parameters α_N^h and α_S^h, related to normal and shear behaviors respectively, like the isotropic elastic tensor.

$$\alpha_{ijkl}^h \equiv \begin{bmatrix} \alpha_N^h & \alpha_N^h-\alpha_S^h & \alpha_N^h-\alpha_S^h & 0 & 0 & 0 \\ \alpha_N^h-\alpha_S^h & \alpha_N^h & \alpha_N^h-\alpha_S^h & 0 & 0 & 0 \\ \alpha_N^h-\alpha_S^h & \alpha_N^h-\alpha_S^h & \alpha_N^h & 0 & 0 & 0 \\ 0 & 0 & 0 & \alpha_S^h & 0 & 0 \\ 0 & 0 & 0 & 0 & \alpha_S^h & 0 \\ 0 & 0 & 0 & 0 & 0 & \alpha_S^h \end{bmatrix} \tag{17}$$

Furthermore, r_{kl} is a symmetric second-order tensor associated with the loading history:

$$r_{kl} = \begin{cases} +1, & \text{if } \sigma_{kl} > 0 \\ 0, & \text{if } \sigma_{kl} = 0 \\ -1, & \text{if } \sigma_{kl} < 0 \end{cases} \tag{18}$$

Considering non-simultaneous multiaxial loadings, the parameter r_{kl} is calculated for the subsequent loadings (assuming stress driving cases), as written below:

$$r_{kl} = \frac{\sigma_{kl}}{|S_{kl}^{\max}|} \text{ if } \beta^+ \neq 0 \text{ or } \beta^- \neq 0 \tag{19}$$

where $S_{kl}^{\max}$ is the maximum value of the mechanical loading that can be a stress or a strain. Moreover, note that $\frac{\sigma_{kl}}{|S_{kl}^{\max}|} = 0$ if $S_{kl}^{\max} = 0$.

Temperature functions, Λ and $\Lambda^{\aleph}$, define the critical stress value for the phase transformation level.

$$\Lambda = 2\Lambda^M = \begin{cases} -L_0^\pm + \dfrac{L^\pm}{T^M}(T - T^M) & \text{if } T > T^M \\ -L_0^\pm & \text{if } T \leq T^M \end{cases} \tag{20}$$

$$\Lambda^{\aleph} = \Lambda^M + \Lambda^A = \begin{cases} -L_0^A + \dfrac{L^A}{T^M}(T - T^M) & \text{if } T > T^M \\ -L_0^A & \text{if } T \leq T^M \end{cases} \tag{21}$$

where T^M is the temperature below which the martensitic phase becomes stable for a stress-free state; Λ^M and Λ^A are the stress phase transformation values for martensite and austenite, respectively.

Moreover, α is a parameter that controls the height of the stress-strain hysteresis loop. The parameters as α, L_o^+, L_o^-, L_o^A, L^+, L^-, L^A, also presents a saturation characteristic as follows:

$$(\ \ ) = (\widehat{\ }) \left[\frac{n + \exp\left(-m^{(\ \ )}\xi^{\pm}\right)}{n+1}\right] \tag{22}$$

where n is used to obtain an appropriate adjustment, and $m^{(\ \ )}$ is a saturation parameter.

Considering the thermoelastic parameters, E_{ijkl} is the elastic tensor; Ω_{ij} is related to the thermal expansion coefficient can be represented by the same general form: $E_{ijkl} = E_{ijkl}^M + \beta^A\left(E_{ijkl}^A - E_{ijkl}^M\right)$; $\Omega_{ij} = \Omega_{ij}^M + \beta^A\left(\Omega_{ij}^A - \Omega_{ij}^M\right)$. Concerning classical plasticity parameters, K is the plastic modulus; H is the kinematic hardening modulus. These parameters can be defined considering a rule of mixture: $K = K^M + \beta^A(K^A - K^M)$ and $\frac{1}{H} = \frac{1}{H^M} + \beta^A\left(\frac{1}{H^A} - \frac{1}{H^M}\right)$. In addition, $\hat{\sigma}_{ij}$ is the deviatoric stress tensor; γ is the plastic multiplier; T_0 is a reference temperature in a stress-free state.

Additionally, η^I defines the coupling between phase transformation and isotropic hardening; η_{ij}^K defines the coupling between phase transformation and kinematic hardening:

$$\eta_{ij}^K \equiv \eta^K \begin{bmatrix} 1 & 1 & 1 \\ 1 & 1 & 1 \\ 1 & 1 & 1 \end{bmatrix} \tag{23}$$

The yield surface is defined by the yield stress σ_Y that has different values for austenitic and martensitic phases.

$$\begin{cases} \sigma_Y = \sigma_Y^M & \text{if } T \le T^M \\ \sigma_Y = \dfrac{\sigma_Y^M(T^A - T) + \sigma_Y^{Ai}(T - T^M)}{T^A - T^M} & \text{if } T^M < T \le T^A \\ \sigma_Y = \dfrac{\sigma_Y^{Ai}(T^F - T) + \sigma_Y^{Af}(T - T^A)}{T^F - T^A} & \text{if } T^M < T \le T^F \end{cases} \tag{24}$$

where T^A is the temperature above which the austenitic phase is stable; T^F is a reference temperature for the determination of the yield stress for high temperatures; σ_Y^M is yield stress of the martensitic phase; σ_Y^{Ai} and σ_Y^{Af} define the thermal variation of the yield stress of the austenitic phase.

The TRIP effect is represented by the parameters M_{13}, M_{31}, M_{23}, M_{32}, M_{34} and M_{43}, defined by $M_{ij} = \widehat{M}_{ij}\exp(-m^M\xi^i)$, where m^M is a saturation parameter. To control the amount of TRIP strain at different temperatures, the following expressions are written:

$$\widehat{M}_{ij} = \begin{cases} 0 & \text{if } T < T^{trip} \\ \widehat{M}_{ij}^R \dfrac{(T - T^{trip})}{(T^F - T^{trip})} & \text{if } T \ge T^{trip} \end{cases} \tag{25}$$

where $\widehat{M}_{ij}^R$ is a reference value of $\widehat{M}_{ij}$ at $T = T^{trip}$ and T^{trip} is a temperature below which TRIP should not occur.

Finally, ω_{ij} and $P^m(m = +, -, A)$ are auxiliary variables. More details about model parameters can be found in Dornelas *et al*. (2021).

Damage description is inspired on the classical theory of continuous damage proposed by Lemaitre and Chaboche (1990). Therefore, the function $(C_1 + C_2\Gamma^\sigma)^{C_3}$ is proposed to define the relationship between accumulated phase transformation and functional damage. Besides, the functions $(C_4 + C_5\Gamma^\sigma)^{C_6}$ and $(C_7 + C_8\Gamma^\sigma)^{C_9}$ are defined to represent the elastic and elastoplastic fatigue, respectively. These functions consider the parameters C_{1-3} to control the evolution of functional damage and C_{4-9} to control the evolution of structural damage. The fatigue life of SMAs is estimated by the constitutive model through the definition of the equivalent critical damage, D_c, that takes into account the effects caused by the functional and structural damage.

$$D_c = [\zeta^A\beta^A + \zeta^+\beta^+ + \zeta^-\beta^-]D_e + D_f \tag{26}$$

where ζ^A, ζ^+ and $\zeta^-$are parameters that represent the austenite and martensite structural fatigue strength. In this sense, the failure occurs when the equivalent critical damage reaches a critical value, D_c^{crit}, which can be calculated through experimental tests.

3. NUMERICAL SIMULATIONS

Initially, this section presents a comparison between numerical simulations and experimental results obtained by Dornelas *et al.* (2021), where a pseudoelastic NiTi SMA wire is subjected to cyclic tension with peak stress ($\sigma_{11}^{\max}$) of 750 MPa, and a frequency of 0.25 Hz. Afterward, numerical simulations are performed to quantify the influence of the peak stress on the loss of actuation performance. Parameters presented in Tab. 1 are employed in all simulations.

Figure 1(a) shows the numerical-experimental comparison considering the first ten cycles. Figure 1(b) shows the numerical-experimental comparison between cycles 1308 – 2308 (experimental) and 1308 – 2284 (last predicted cycles). The TRIP strain and the accumulation of functional and structural damage promote a loss of actuation performance with the increase of the number of cycles. It should be pointed out the good agreement between numerical and experimental results, showing the model capability to describe the evolution of TRIP strain and fatigue during the cyclic loading process.

Figure 2(a) shows the evolution of dissipated energy per unit volume (MJ/ m^3). This functional parameter quantifies the material's ability to dissipate energy during the phase transformation process. The first cycles are essentially characterized by the stabilization of the TRIP strain, where a reduction in the hysteresis loop occurs. This aspect can be observed in Fig. 2(a), where a reduction of the dissipated energy from 10.5 (MJ/ m^3) to approximately 4.5 (MJ/ m^3) takes place. After this point, there is a reduction of the dissipated energy throughout the cycles due to the evolution of functional and structural fatigue. During the loading process, there is approximately 70% of dissipated energy. Figure 2(b) shows the evolution of the maximum value of austenite volume fraction during the cyclic loading process. In the first cycles, the material has 100% of its performance capacity, and this percentage progressively decreases due to the evolution of damage, until reaching approximately 60% in the last cycle before the failure.

Table 1. **Parameters identified from experimental results performed by Dornelas *et al.* (2021).**

E^A (GPa)	E^M (GPa)	Ω^A (MPa/K)	Ω^M (MPa/K)	α_N^h (MPa)	$\hat{\alpha}$ (MPa)
58.0	36.0	0.74	0.17	0.028	100.0
$\hat{L}_0^{\pm}$ (MPa)	$\hat{L}^{\pm}$ (MPa)	$\hat{L}_0^A$ (MPa)	$\hat{L}^A$ (MPa)	$(\eta_L)_N$ (MPa. s)	$(\eta_U)_N$ (MPa. s)
6.00	5.00	0.60	105.50	0.10	0.80
$(\eta_L^A)_N$ (MPa. s)	$(\eta_U^A)_N$ (MPa. s)	T^M (K)	T^A (K)	T_0(K)	σ_Y^M (GPa)
0.10	0.80	266.0	297.0	300.0	0.30
σ_Y^{Ai} (GPa)	σ_Y^{Af} (GPa)	K^A (GPa)	K^M (GPa)	H^A (GPa)	H^M (GPa)
1.15	0.60	1.4	0.4	4.0	1.1
η^I	η^K	T^F (K)	$\widehat{M}_{13}$ (GPa^{-1})	$\widehat{M}_{31}$ (GPa^{-1})	$\widehat{M}_{32}$(GPa^{-1})
–0.01	–0.01	423.0	0.85	0.05	0.85
$\widehat{M}_{23}$ (GPa^{-1})	T^{trip}(K)	m^{α}	m^L	m^M	n
0.05	297.0	1.0×10^{-4}	0.1	0.4	0.7
C_1	C_2	C_3	C_4	C_5	C_6
5.0×10^{-6}	5.5×10^{-12}	1.58	5.0×10^{-12}	8.9×10^{-12}	1.58
ζ^A	ζ^+	D_c^{crit}			
3.38	0.87	0.16			

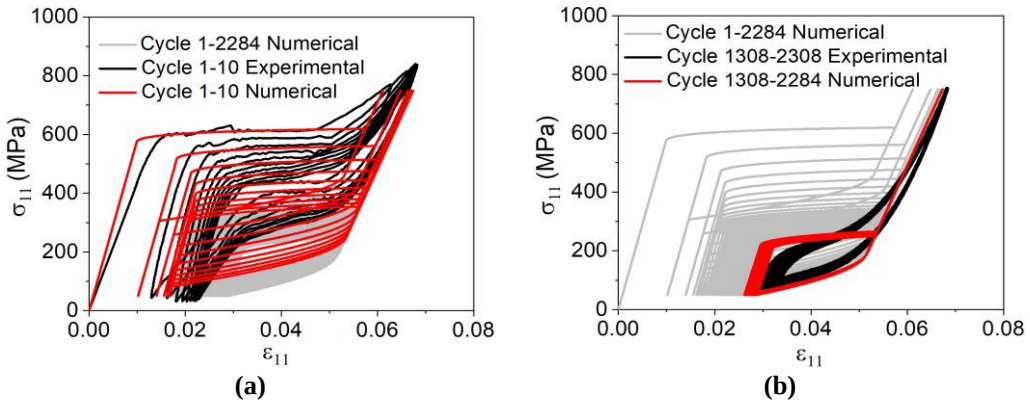

Figure 1. **Pseudoelastic behavior for NiTi wires during fatigue tests, Dornelas *et al.* (2021), $\sigma_{11}^{\max} = 750$ MPa, 0.25 Hz. Numerical-experimental comparative for different cycles: (a) cycle 1 – 10; (b) cycle 1308 – 2308 (experimental) and cycle 1308 – 2284 (numerical).**

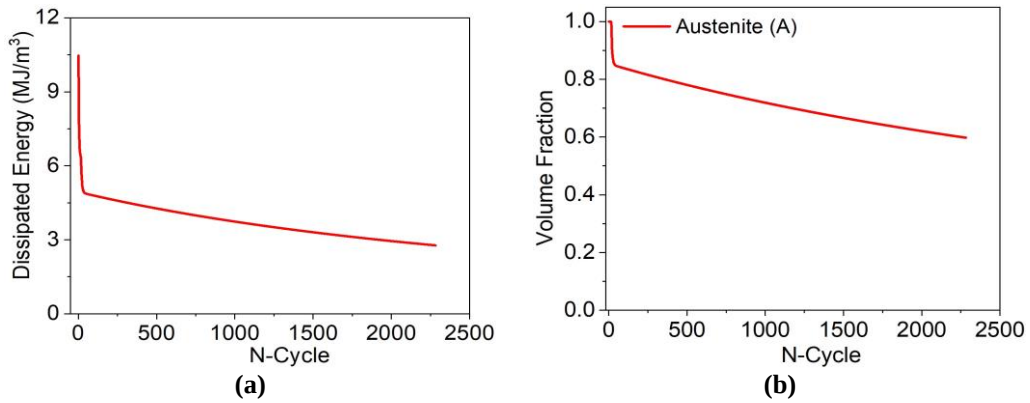

Figure 2. **Loss of actuation performance. (a) dissipated energy evolution; (b) maximum value of austenite volume fraction during cyclic loading.**

Figure 3(a) presents the evolution of TRIP strain during the first 50 cycles showing that the material undergoes a rapid stabilization, around 10 cycles. Figure 3(b) presents the evolution of functional and structural damage. After 2284 cycles, the functional damage reaches a value of approximately 12%, causing the loss of actuation performance. On the other hand, the structural damage reaches a value of approximately 2% in the last cycle before the rupture. Finally, Fig. 3(c) shows the evolution of critical damage over the cycles until reaching $D_c^{crit} = 0.16$. By considering the numerical-experimental comparison, it should be pointed out that there was a good fatigue life prediction with a variation of 1% between experimental tests and results predicted by the model.

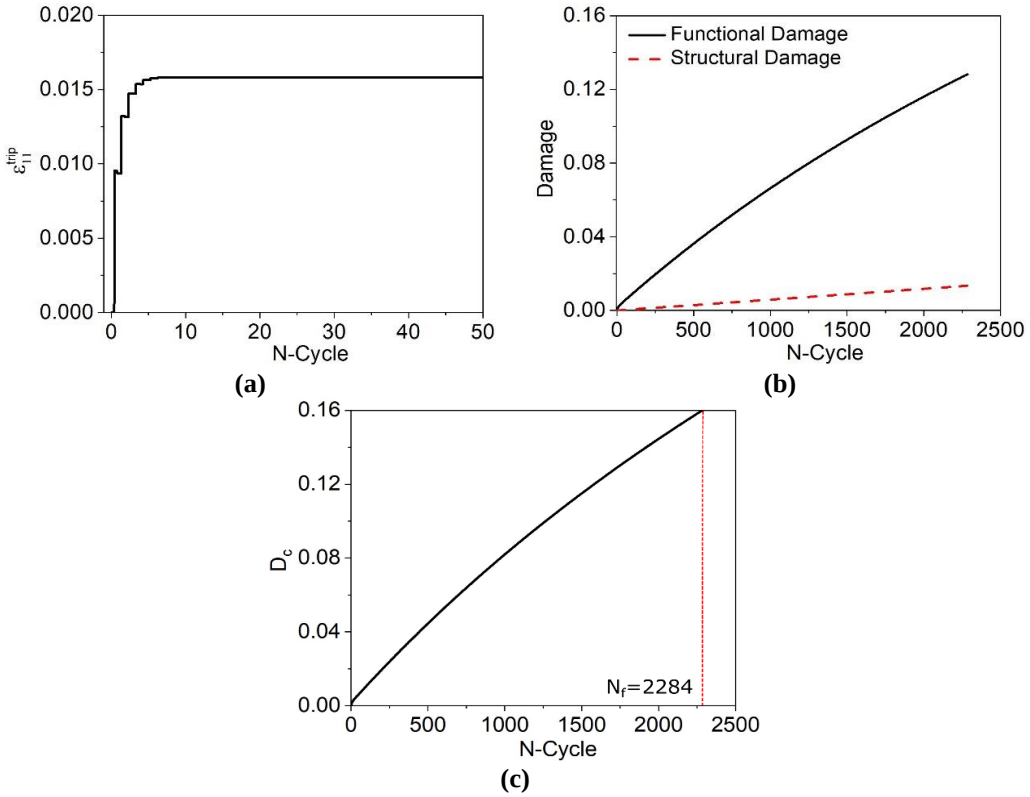

Figure 3. **TRIP strain and damage evolution during fatigue tests. (a) TRIP evolution; (b) functional and structural damage evolution; (c) critical damage evolution.**

The influence of the peak stress on the loss of actuation performance is now of concern considering two numerical simulations with a frequency of 0.25 Hz and different peak stress values. Two thousand cycles are analyzed in both tests. Figures 4(a), (c), (e), and (g) present results obtained for $\sigma_{11}^{max} = 650$ MPa and Figs. 4(b), (d), (f), and (h) consider results obtained for $\sigma_{11}^{max} = 950$ MPa.

Figures 4 (a) and (b) present the stress-strain curves showing that the increase of the applied stress is associated with a stabilization of the TRIP strain that promotes a greater loss of performance during the first cycles, and there is a greater reduction of the hysteresis loop in the last cycle due to the loss of material functionality. Figures 4(c) and (d) show the

evolution of dissipated energy per unit volume (MJ/ m^3), where it is observed that increasing the applied stress, a more pronounced decrease of the dissipated energy capacity occurs.

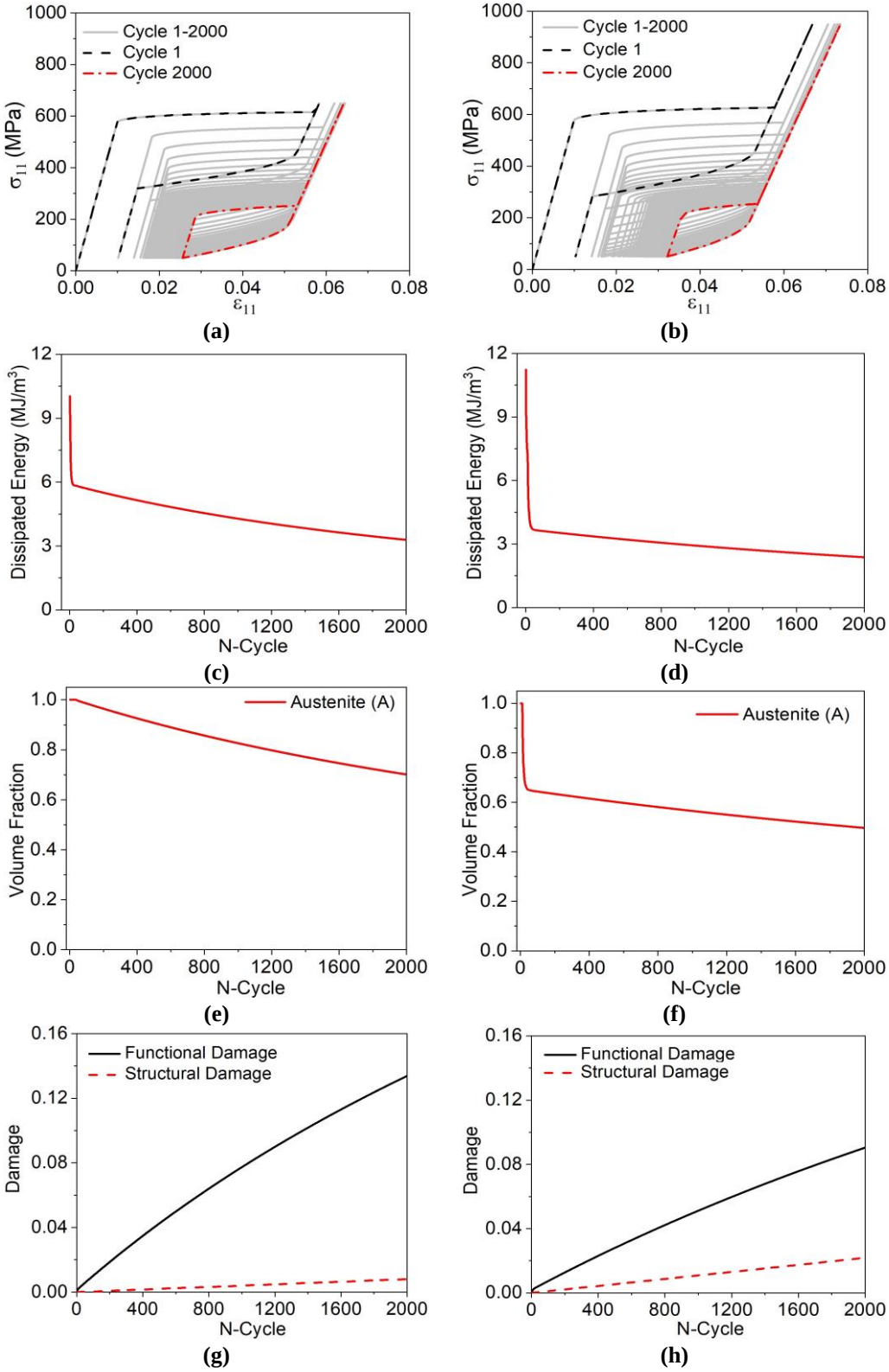

Figure 4. **Influence of the peak stress on the loss of actuation performance. (a) stress-strain evolution, $\sigma_{11}^{max} = 650$ MPa; (b) stress-strain evolution, $\sigma_{11}^{max} = 950$ MPa; (c) dissipated energy evolution, $\sigma_{11}^{max} = 650$ MPa; (d) dissipated energy evolution, $\sigma_{11}^{max} = 950$ MPa; (e) maximum value of austenite volume fraction, $\sigma_{11}^{max} = 650$ MPa; (f) maximum value of austenite volume fraction, $\sigma_{11}^{max} = 950$ MPa; (g) functional and structural damage evolution, $\sigma_{11}^{max} = 650$ MPa; (h) functional and structural damage evolution, $\sigma_{11}^{max} = 950$ MPa.**

Figures 4(e) and (f) present the evolution of the maximum value of austenite volume fraction during the cyclic loading process. Initially, it is observed that the material has 100% of its phase transformation capacity for both applied loading. After a few cycles, a rapid decrease of the phase transformation capacity of the material subjected to $\sigma_{11}^{\max} = 950$ MPa take place. Considering the last cycle of the test, the material subjected to $\sigma_{11}^{\max} = 650$ MPa has 70% of its phase transformation capacity. On the other hand, the material subjected to $\sigma_{11}^{\max} = 950$ MPa has approximately 50% of its phase transformation capacity. This result indicates that by increasing the applied stress from 650 MPa to 950 MPa, keeping the same test conditions, the material loses approximately 20% of its phase transformation capacity.

Finally, Figs. 4(h) and (g) show the evolution of functional and structural damage. Note that the increase of the applied stress promotes a more severe functional property change in the first cycles of the test, promoting a reduction of the rate of evolution of functional damage. On the other hand, the increase of applied stress promotes a more pronounced accumulation of structural damage.

4. CONCLUSIONS

This paper presents a numerical investigation of the influence of functional and structural fatigue of shape memory alloys. The three-dimensional model proposed by Dornelas *et al.* (2021) is employed to perform numerical simulations. Initially, numerical results are compared with experimental data considering a cyclic tension test. It is observed that the TRIP strain associated with the functional and structural damage promotes a loss of actuation performance with the increase of the number of cycles. Results show that the model responses are in close agreement with experimental data, including fatigue life predictions. After the model verification, numerical simulations considering different levels of peak stress are proposed to evaluate the degradation of the functional aspects. Results show that the increase of the peak stress promotes a more pronounced loss of actuation performance of the material due to the evolution of the TRIP strain and fatigue. Numerical results are qualitatively similar to experimental data available in the literature, confirming the model capability to describe the SMA fatigue phenomenon.

5. ACKNOWLEDGEMENTS

The authors would like to acknowledge the support of the Brazilian Research Agencies CNPq, CAPES, and FAPERJ.

6. REFERENCES

Barrera, N., Biscari, P., Urbano, M.F., 2014. “Macroscopic modeling of functional fatigue in shape memory alloys”. *European Journal of Mechanics - A/Solids*, Vol. 45, pp. 101–109.

Chemisky, Y., Hartl, D.J., Meraghni, F., 2018. “Three-dimensional constitutive model for structural and functional fatigue of shape memory alloy actuators”. *International Journal of Fatigue*, Vol. 112, pp. 263–278.

Dornelas, V.M., Oliveira, S.A., Savi, M.A., 2020. “A macroscopic description of shape memory alloy functional fatigue”. *International Journal of Mechanical Sciences*, Vol. 170, pp. 105345.

Dornelas, V.M., Oliveira, S.A., Savi, M.A., Pacheco, P.M.C.L., De Souza, L.F.G., 2021. “Fatigue on shape memory alloys: Experimental observations and constitutive modeling”. *International Journal of Solids and Structures*, Vol. 213, pp. 1–24.

Eggeler, G., Hornbogen, E., Yawny, A., Wagner, M., 2004. “Structural and functional fatigue of NiTi shape memory alloys”. *Materials Science and Engineering*, Vol. 378, pp. 24–33.

Halphen, B. and Nguyen, Q.S., 1975. Sur les matériaux standard généralisés. *Journal de Mécanique*, Vol. 14, pp. 39–63.

Hartl, D.J. and Lagoudas, D.C., 2007. “Aerospace applications of shape memory alloys”. In *Proceedings of the Institution of Mechanical Engineers, Part G: Journal of Aerospace Engineering*, Vol. 221, No. 4, pp. 535–552.

Hartl, D.J., Chemisky, Y., Meraghni, F., 2014. “Three-dimensional constitutive model considering transformation-induced damage and resulting fatigue failure in shape memory alloys”. In *SPIE Smart Structures and Materials + Nondestructive Evaluation and Health Monitoring*, *International Society for Optics and Photonics*. San Diego, CA, USA, pp. 905805.

Jani, J.M., Leary, M., Subic, A., Gibson, M.A., 2014. “A review of shape memory alloy research, applications and opportunities”. *Materials and Design*, Vol. 56, pp. 1078–1113.

Jaureguizahar, S.M., Chapetti, M.D., Yawny, A., 2018 A novel experimental method to assess the fatigue behavior of pseudoelastic NiTi wires. *International Journal of Fatigue*, Vol. 116, pp. 300–305.

Kang, G., Kan, Q., Yu, C., Song, D., Liu, Y., 2012. “Whole-life transformation ratchetting and fatigue of super-elastic NiTi Alloy under uniaxial stress-controlled cyclic loading*”. Materials Science and Engineering A*, Vol. 535, pp. 228–234.

Lemaitre, J. and Chaboche, J.L., 1990, *Mechanics of Solid Materials*. Cambridge University Press: Cambridge, UK, ISBN 9780521328531.

Liu, B., Chen, K., Zhou, R., 2020a. “Damage evolution and fatigue life prediction of the shape memory alloy under low cycle fatigue”. *Materials Today Communications*, Vol. 26, pp. 101636.

Liu, B., Jin, S., Li, X., Zhou, R., 2020b. “Study on behaviors of shape memory alloy materials under temperature cycling considering the damage”. J. *Journal of Intelligent Material Systems and Structures*, Vol. 31, pp. 990–997.

Machado, L.G. and Savi, M.A., 2003. “Medical applications of shape memory alloys”. *Brazilian Journal of Medical and Biological Research*, Vol. 36, pp. 683–691.

Mohammadzadeh, M.R., Kadkhodaei, M., Barati, M., Chirani, S.A., Saint-Sulpice, L., 2019. “Modeling of torsion fatigue in shape memory alloys”. *Journal of Intelligent Material Systems and Structures*. Vol. 30, pp. 3146–3162.

Nematollahi, M., Baghbaderani, K.S., Amerinatanzi, A., Zamanian, H., Elahinia, M., 2019. “Application of NiTi in assistive and rehabilitation devices: A review”. *Bioengineering*, Vol. 6, pp. 37.

Oliveira, S.A., Savi, M.A., Zouain, N., 2016. “A three-dimensional description of shape memory alloy thermomechanical behavior including plasticity”. *Journal of the Brazilian Society of Mechanical Sciences and Engineering*., Vol. 38, pp. 1451–1472.

Oliveira, S.A., Dornelas, V.M., Savi, M.A., Pacheco, P.M.C.L., Paiva, A., 2018. “A phenomenological description of shape memory alloy transformation induced plasticity”. *Meccanica*, 53, 2503–2523.

Petrini, L. and Bertini, A., 2020. “A three-dimensional phenomenological model describing cyclic behavior of shape memory alloys”. *International Journal of Plasticity*, Vol. 125, pp. 348–373.

Phillips, F.R., Wheeler, R.W., Geltmacher, A.B., Lagoudas, D.C., 2019. “Evolution of internal damage during actuation fatigue in shape memory alloys”. *International Journal of Fatigue*, Vol. 124, pp. 315–327.

Predki, W., Klönne, M., Knopik, A., 2006. “Cyclic torsional loading of pseudoelastic NiTi shape memory alloys: Damping and fatigue failure”. *Materials Science Engineering: A*, Vol. 417, pp. 182–189.

Qin, X., Zhang, X., Yan, X., Wang, S., Zhang, S., Guo, C., Jiang, J., Zhang, B., Huang, D., Qi, M., 2019. “Structural and functional fatigue behavior of Ni 49.8 Ti 50.2 (at.%) wires under various maximum heating temperatures: Experimental and modeling study”. *Materials & Design*, Vol. 178, pp. 107842.

Qiu, B., Kan, Q., Kang, G., Yu, C., Xie, X., 2019. “Rate-dependent transformation ratcheting-fatigue interaction of super-elastic NiTi alloy under uniaxial and torsional loadings: Experimental observation”. *International Journal of Fatigue*, Vol. 127, pp. 470–478.

Ramos, A.D.O., De Araújo, C.J., De Oliveira, H.M.R., Macêdo, A., Lima, A.G.B., 2018. “An experimental investigation of the super-elastic fatigue of NiTi SMA wires”. *Journal of the Brazilian Society of Mechanical Sciences and Engineering*, Vol. 40, pp. 206.

Tyc, O., Heller, L., Vronka, M., Sittner, P., 2020. “Effect of temperature on fatigue of superelastic NiTi wires”. *International Journal of Fatigue*, Vol. 134, pp. 105470.

Zhao, T., Kang, G., Yu, C., Kan, Q., 2020. “Experimental study on whole-life one-way shape memory cyclic degradation and fatigue failure of NiTi shape memory alloy”. *Materials Today Communications*, Vol. 25, pp. 101621.

7. CONFLICTS OF INTEREST

The authors declared no potential conflict of interest with respect to the research, authorship, and/or publication of this article.